9

Research article

Shirong Lin, Zhongquan Nie*, Weichao Yan, Yao Liang, Han Lin, Qing Zhao* and Baohua Jia*

All-optical vectorial control of multistate magnetization through anisotropy-mediated spin-orbit coupling

https://doi.org/10.1515/nanoph-2019-0198 Received June 27, 2019; revised August 23, 2019; accepted September 10, 2019

Abstract: The interplay between light and magnetism is considered as a promising solution to fully steer multidimensional magnetic oscillations/vectors, facilitating the development of all-optical multilevel recording/memory technologies. To date, impressive progress in multistate magnetization instead of a binary level has been witnessed by primarily resorting to double laser beam excitation. Yet, the control mechanisms are limited to specific magnetic medium or intricate optical configuration as well as overlooking the crystallographic architecture of the media and the polarization-phase linkage of the light fields. Here, we theoretically present a novel all-optical strategy for generating arbitrary multistate magnetization through the inverse Faraday effect. This is achieved by strongly focusing a single vortex-phase configured beam with circular

polarization onto the anisotropic magnetic medium. By judiciously tuning the topological charge effect, the optical anisotropic effect, and the anisotropic optomagnetic effect, the light-induced magnetic vector can be flexibly redistributed between its transverse and longitudinal components, thus enabling orientation-unlimited multilevel magnetization control. In this optomagnetic process, we also reveal the role of anisotropy-mediated spin-orbit coupling, another physical mechanism that enables the effective translation of the angular momentum of light fields to the magnetic system. Furthermore, the conceptual paradigm of all-optical multistate magnetization is verified. Our findings show great prospect in multidimensional high-density optomagnetic recording and memory devices and also in high-speed information processing science and technology.

Keywords: anisotropic media; inverse Faraday effect; optomagnetic effect; spin-orbit coupling; structured beams.

*Corresponding author: Zhongquan Nie, Key Laboratory of Advanced Transducers and Intelligent Control System, Ministry of Education and Shanxi Province, Taiyuan 030024, China; and College of Physics and Optoelectronics, Taiyuan University of Technology, Taiyuan 030024, China, e-mail: niezhongquan1018@163.com, Qing Zhao Center for Quantum Technology Research, School of Physics, Beijing Institute of Technology, Beijing 100081, China, e-mail: qzhaoyuping@bit.edu.cn; and Baohua Jia Centre for Translational Atomaterials, Faculty of Science, Engineering and Technology, Swinburne University of Technology, Hawthorn, Victoria 3122, Australia, e-mail: bjia@swin.edu.au. https://orcid.org/0000-0002-6703-477X

Shirong Lin: Center for Quantum Technology Research, School of Physics, Beijing Institute of Technology, Beijing 100081, China; and Centre for Translational Atomaterials, Faculty of Science, Engineering and Technology, Swinburne University of Technology, Hawthorn, Victoria 3122, Australia

Weichao Yan: Centre for Translational Atomaterials, Faculty of Science, Engineering and Technology, Swinburne University of Technology, Hawthorn, Victoria 3122, Australia; and Department of Physics, Harbin Institute of Technology, Harbin 150001, China Yao Liang and Han Lin: Centre for Translational Atomaterials, Faculty of Science, Engineering and Technology, Swinburne University of Technology, Hawthorn, Victoria 3122, Australia

1 Introduction

In conventional magnetism, magnetic memories rely largely on the bistability of the magnetization vector in magnetic materials [1–4]. Specifically, traditional magnetic memory devices involve a binary process in which the logical bits, magnetization states, can be either "up" or "down". The demand for the ever-growing vast density of magnetic storage, however, has triggered a new upsurge for avenues to attain multilevel states in these magnetic systems. Tremendous research endeavors in this regard, embracing ingenious magnetic characteristic or resistance switching design, have been devoted toward multiplexing the magnetization/resistance into diverse levels with a controllable polarization orientation [5–8]. Despite extensive effects and significant progresses, it is still challenging to resolve the limited states, slow switching speed and low-energy efficiency issues dictated by external electrical or magnetic fields.

In contrast, optical pulses are rapidly emerging as a viable top-notch tool for fast and rich manipulation of magnetization via the canonical inverse Faraday effect (IFE) [9–14], wherein the magnetization scale, orientation, and pattern of each magnetic domain can be controlled in principle with the illumination of delicate phase, polarization, and angular momentum (AM) of the configured light beams. In this context, it is feasible to access numerous versatile magnetization architectures with longitudinal [15, 16] or transverse [17] polarizations. Of particular intriguing application of these optomagnetic controls is the all-optical magnetic recording/storage, whereas magnetization vectors in these scenarios remain limited to a binary process.

Designing maximalist discrete levels in a magnetic system is of crucial importance, as the recording density and storage volume of any magnetic memory device initiated by the tailored light fields is intimately related to the amount of magnetized states. To pursue this goal, it has been experimentally demonstrated that all-optical control of two-dimensional (2D) or three-dimensional (3D) magnetic oscillation eigenstates in selective antiferromagnet could represent a performable alternative [18, 19]. More impressively, by leveraging the prescribed vectorial beams, a forward numerical approach in a 4π optical microscopic configuration and a reverse analytical method with dipole antenna theory are proposed to yield magnetization with tunable 3D polarized orientations in isotropic nondissipative magneto-optical materials [20, 21]. The preliminary progresses based on the aforementioned proof-of-concepts open up new vistas on high-density nonbinary information recording and storage devices. However, they may suffer from serious practical limitations due to the complexity of aligning the double optical paths, the specificity of selecting magnetic media, and the neglect of crystallographic structures of the media and the spin-orbit coupling (SOC) of the light fields.

Here, we theoretically introduce a viable all-optical methodology, named anisotropy-mediated SOC, to create multiple magnetization states, in which we not only take the axial birefringence effect of the magnetooptical medium into account but also draw polarizationphase synergy of incident beams into the optomagnetic system. Under these circumstances, the light-induced magnetic vector can be arbitrarily redistributed between its transverse component and longitudinal component, thus making an orientation-unlimited multilevel magnetization control possible in principle. Delving deep into the optomagnetic interaction with optical SOC, we identify the transfer of AM from the light fields to the material system by virtue of the topological charge effect, the optical anisotropic effect, and the anisotropic optomagnetic effect. The interactions between configured light beams and anisotropic magnetism provide comprehensive physical insights for modern magnetism. Apart from fundamental interests, multistate polarized magnetization underpins broad applications such as multidimensional high-density all-optical magnetic recording and memory as well as high-speed information processing.

2 Theoretical framework

2.1 IFE under tight focusing conditions

We investigated the generation and control of vectorial and multilevel magnetization states by the interaction of the vortex-encoded vectorial beam with circular polarization and the anisotropic magneto-optical material. The configuration of this idea is shown in Figure 1. In isotropic medium 1, such as the materials in the solid immersion lens system, an incident structured light is first collected by a high numerical aperture (NA) objective lens and then tightly focused towards the interface at z=-d, refracting into the anisotropic nonabsorbing magneto-optical medium 2, at the focal plane z=0, in which there will be optically stimulated magnetization excitation via the IFE. In particular, the structured light is circularly polarized with helical phase wavefront described by $\Psi(\phi) = \exp(im\phi)$, where ϕ is the azimuthal coordinate in the transverse plane and *m*

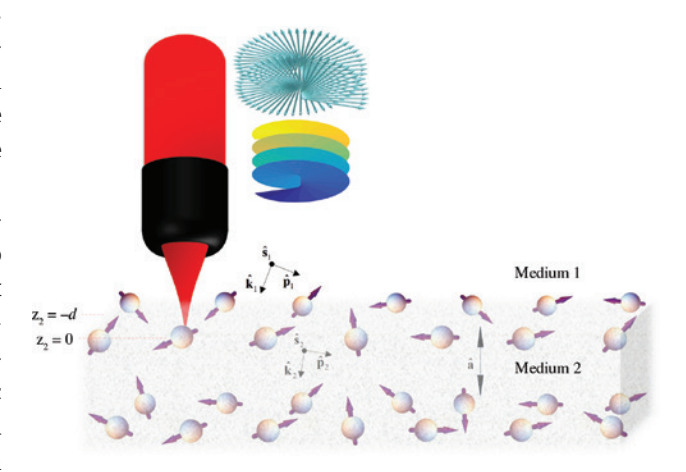


Figure 1: (Color online) Scheme for the optomagnetic recording via the IFE under tight focusing condition, with refraction at the interface in z = -d and focal plane in z = 0; $\hat{\mathbf{k}}_1$ and $\hat{\mathbf{k}}_2$ are unit wave vectors in media 1 and 2, respectively; $\hat{\mathbf{s}}_1$, $\hat{\mathbf{p}}_1$ and $\hat{\mathbf{s}}_2$, $\hat{\mathbf{p}}_2$ are the associated unit polarization vectors perpendicular and parallel to the plane of incidence, respectively. Medium 2 is characterized by the uniaxial symmetry axis \hat{a} perpendicular to the interface.

is the topological charge. Light fields in media 1 and 2 are parameterized by wave vectors $\hat{\mathbf{k}}_{1,2}$ and polarization vectors $\hat{\mathbf{s}}_{1,2}$ and $\hat{\mathbf{p}}_{1,2}$. These unit vectors form orthonormal sets, i.e. $\hat{\mathbf{p}}_{1,2} \times \hat{\mathbf{s}}_{1,2} = \mathbf{k}_{1,2}$. The high NA objective focusing geometry allows achieving the smallest possible focal spot, thus yielding a high-resolution magnetization pattern.

Here, we consider the axially birefringent medium with uniaxial symmetry axis $\hat{\mathbf{a}}$ along the optical axis (zaxis). In the principal axes frame, this medium is characterized by the relative permittivity as $\hat{\epsilon} = \text{diag}(n_a^2, n_a^2, n_a^2)$, where n_{a} and n_{b} denote the ordinary and extraordinary refractive indices, respectively. The difference between them is referred to as birefringence, $\Delta n = |n_0 - n_0|$.

Generally, intensive light with circular polarization travelling into a nonabsorbing material induces an effective magnetic field, thereby leading to the corresponding magnetization $M_k(0) = \chi_{ijk} E_i(\omega) E_j^*(\omega) = i e_{ijl} \gamma_{lk} E_i(\omega) E_j^*(\omega)$ [22], where e_{ii} is the 3D Levi-Civita symbol, third-rank tensor χ_{iik} and second-rank tensor γ_{ν} are the optomagnetic susceptibilities, $\mathbf{E}(\omega)$ is the electric field of the light, and asterisks are the complex conjugates. This nonthermal optomagnetic effect, IFE, is a nonlinear optical effect or a linear inverse magneto-optical phenomenon. Microscopically, the IFE is a stimulated Raman-like coherent optical scattering process. High-intensity light fields of elliptical or circular polarization shift the magnetic ground states and combine these ground states with some excited states, eventually giving rise to the light-induced magnetization [23–25]. The IFE has been investigated in various natural and artificial materials, including diamagnetic, paramagnetic, ferromagnetic, ferromagnetic, and antiferromagnetic systems in dielectrics, semiconductors, and metals, covering both amorphous and crystalline structures [11, 13, 14, 26-28]. Here, we consider the IFE in the anisotropic dielectric medium, which can be paramagnetic crystals [29] or magnetically ordered crystals in their paramagnetic or diamagnetic phases [13, 26, 30–32]. Dielectric medium is the promising candidate for the applications via ultrafast optomagnetic process as the thermal effects caused by an intense laser irradiation occur only in the nanosecond range [13]; thus, the thermal effects can be neglected in our discussion. It is worth mentioning that in anisotropic medium γ_n is generally a second-order tensor. That is, the optomagnetic response is generally anisotropic as well [33–36].

The sharp focusing beam in the focal region within the anisotropic medium can be numerically calculated by the Debye diffraction method [37-40]. Owing to the optical anisotropy, the incident light will split into two eigenmodes in the birefringent medium. We pay attention only to the anisotropic medium with small birefringence so that the radially extraordinary (p) and tangentially

ordinary (s) modes are still combined to form a single focal spot, which is vital to many applications especially for the all-optical magnetic recording. In this situation, the refractive index of the axially birefringent medium, medium 2 in Figure 1, can be approximately represented by n_0 . Therefore, the electric field in the focal region of this axially birefringent dielectric can be expressed as $E(r_2) = E^p(r_2) + E^s(r_2)$ [41] (see details of the derivations in Section 1 of Supplementary Material):

$$\begin{pmatrix}
E_{x}^{p} \\
E_{y}^{p} \\
E_{z}^{p}
\end{pmatrix} = \int_{0}^{\alpha} d\theta_{1} \sin \theta_{1} \sqrt{\cos \theta_{1}} e^{ik_{2}z_{2}\cos \theta_{2}}$$

$$\begin{pmatrix}
\cos \theta_{2} \left(-iI_{m}^{p} - \frac{i}{2}(\sigma + 1)I_{m+2}^{p} + \frac{i}{2}(\sigma - 1)I_{m-2}^{p}\right) \\
\cos \theta_{2} \left(\sigma I_{m}^{p} - \frac{1}{2}(\sigma + 1)I_{m+2}^{p} - \frac{1}{2}(\sigma - 1)I_{m-2}^{p}\right) \\
i\sin \theta_{2}((1 + \sigma)I_{m+1}^{p} + (1 - \sigma)I_{m-1}^{p})
\end{pmatrix}, (1)$$

and

$$\begin{pmatrix}
E_{x}^{s} \\
E_{y}^{s} \\
E_{z}^{s}
\end{pmatrix} = \int_{0}^{\alpha} d\theta_{1} \sin \theta_{1} \sqrt{\cos \theta_{1}} e^{ik_{2}z_{2}\cos \theta_{2}}$$

$$\begin{pmatrix}
-iI_{m}^{s} + \frac{i}{2}(\sigma + 1)I_{m+2}^{s} - \frac{i}{2}(\sigma - 1)I_{m-2}^{s} \\
\sigma I_{m}^{s} + \frac{1}{2}(\sigma + 1)I_{m+2}^{s} + \frac{1}{2}(\sigma - 1)I_{m-2}^{s} \\
0
\end{pmatrix}, (2)$$

where
$$I_q^l = t_l e^{iW_l} i^q e^{iq\phi} J_q(k_1 r_1 \sin \theta_1); \ l = p, s; \ q = m, m \pm 1, m \pm 2.$$

 α determined by NA = $n_1 \sin \alpha$ is the maximal half-angle of the cone of light that exits the objective lens, where n_i is the refractive index of medium 1. θ_1 denotes the incident angle and θ_2 denotes the refraction angle. J_q is the qth-order Bessel function of the first kind. $t_{\scriptscriptstyle p}$ and $t_{\scriptscriptstyle s}$ are the transmission coefficients for the p and s polarizations, respectively. σ represents the states of polarization of the circularly polarized light, which is either 1 or -1. The dynamical phases of the p and s components introduced in this anisotropic medium are W_n and W_s , respectively. They are considered as aberrations $W_n = \exp(ik_0(d+z_2)\Delta n)$ and $W_s = 0$, where we have assumed that the focusing systems are corrected for spherical aberrations caused by the mismatch in the interface between media 1 and 2. Physically, W_n accounts for the influence of the birefringence and causes distortion and broadening of the focal spot. In our simulations, NA = 1.4, d is equal to 10 times of the wavelength, and n, is set to 1.514 and n_0 to 1.655; we only consider left-circularly polarized

vortex light (σ =1). We emphasize that, in addition to circularly polarized beams, linearly polarized light fields and generalized cylindrical vectorial beams can also be used to achieve comparable effects, as these polarized vortex beams generally result in mixture of both extraordinary (p)and ordinary (s) modes in the focal region.

Accordingly, light-induced magnetization can be calculated by the focal electric fields via the IFE as

$$\mathbf{M} = \begin{pmatrix} M_{x} \\ M_{y} \\ M_{z} \end{pmatrix} = i \begin{pmatrix} \gamma_{xx} (E_{y} E_{z}^{*} - E_{z} E_{y}^{*}) \\ \gamma_{yy} (E_{z} E_{x}^{*} - E_{x} E_{z}^{*}) \\ \gamma_{zz} (E_{x} E_{y}^{*} - E_{y} E_{x}^{*}) \end{pmatrix}$$

$$\equiv i \gamma_{xx} \begin{pmatrix} E_{y} E_{z}^{*} - E_{z} E_{y}^{*} \\ E_{z} E_{x}^{*} - E_{x} E_{z}^{*} \\ \gamma (E_{x} E_{y}^{*} - E_{y} E_{x}^{*}) \end{pmatrix}. \tag{3}$$

For uniaxial medium with time reversal invariance, there are just two independent elements in γ_{lk} : $\gamma_{xx} = \gamma_{vy}$ and γ_{∞} , which is uniquely determined by its crystallographic point group [42]. Briefly, we have used the ratio $\gamma = \gamma_{xx}/\gamma_{xx}$ to characterize the relative ratios of strengths of the optomagnetic responses in different directions. Because of the anisotropy, it is anticipated to further manipulate the magnetization via the anisotropic optomagnetic property by selecting well-behaved media or even changing the material structure to enhance or suppress the optomagnetic response for a suitable γ . Although the anisotropic optomagnetic process is not relevant to the focused electric diffraction pattern, it has a direct impact on the IFE process.

It should be pointed out that in our calculations the maximal value of Δn is 0.03, in which the focal spot does not form a perfectly symmetric pattern but is still a combined one. In this case, it shows some abnormal effects on the light-induced magnetization compared to the smaller Δn cases, which is caused by the broadening of the focal spot (see Section 2 of Supplementary Material for more details).

2.2 Optical SOC in axially birefringent medium

Notably, the optical anisotropy results in the redistribution of the spin AM (SAM) and the orbital AM (OAM) of the electric field in the focal region, as manifested in the E_z component of Eq. (1). It is well known that light generally carries AM, and SAM and OAM are different forms of AM, which relates to different degrees of freedom of the light fields, the polarization and spatial structure, respectively. Nevertheless, there will be SOC, that is, spin-orbit interactions between the polarization and the wavefront of the

light fields, when the light interacts with an optically inhomogeneous and anisotropic material [43, 44] or is tightly focused into the homogeneous and isotropic material [45, 46]. Hence, it is very interesting to explore the magnetization behaviors in the anisotropic material via the IFE in the tight focusing setting. The polarization and the phase structure of the light fields, the optical anisotropy and the anisotropic optomagnetic response of the material, together with the optical SOC mechanism, will provide more degrees of freedom to steer the magnetization vector. Here, due to different focusing behaviors of the p and scomponents in the birefringent medium, we also point out that this coupling occurs only in the p component of the circular polarization as $E_s^s = 0$ in the focal region. Thus, the spin-orbit interaction in the focal region significantly determines the local energy distribution. For example, optical SOC under the condition of $\sigma = \pm 1$ and $m = \pm 1$ leads to a bright spot in the center of the E_z component, as the intensity component $I_z \propto |J_0|^2$; for all other SOC conditions, however, I_z turns out to be doughnut shaped.

The physical consequences of this kind of optical SOC can also be understood when we study the light-induced magnetization in dielectric medium, especially in medium with anisotropic optical and optomagnetic response. Also, note that E appears in the transverse part of **M** (Mand *M*) so that the optical SOC will shape the distribution of **M** in this physical system in a way different from the previous one.

Clearly, the magnetization is explicitly dependent on the incident circularly polarized light structure represented by the topological charge m as well as the magneto-optical material architecture by the birefringence Δn and the anisotropic optomagnetic response γ . Naturally, it is intuitive to simultaneously use these three variables in light and material to vectorially control the magnetization with the help of the optical SOC. Their impacts upon the generation of the magnetization can be estimated by numerically solving Eqs. (1–3).

3 Topological charge effect, optical anisotropic effect, and anisotropic optomagnetic effect

3.1 Influence of light fields

One of the salient features of the light fields is the phase structure. To test the influence of a light field on the magnetization, we consider the case with varied topological

charge for a given material. To quantify the light-induced magnetic energy density distribution, we decompose the magnetization \mathbf{M} into the transverse part $\mathbf{M}_t = \mathbf{M}_x + \mathbf{M}_y$ and the longitudinal part \mathbf{M}_z .

The impact of the topological charge on the magnetization distribution is revealed by considering three cases of different topological charges with both fixed Δn and γ . Figure 2A–C shows the magnetization strength at the focal plane (x-y plane). As one can see, the light-induced \mathbf{M} in this medium can be affected by adjusting light fields with different topological charges. When m=0, the orientation of \mathbf{M} stays at the vertical direction (Figure 2A). In contrast, when OAM is introduced into the light fields, this kind of AM tends to rotate the magnetization toward the horizontal direction (Figure 2B and C). It is expected that if m is large enough, \mathbf{M} will finally locate itself in the horizontal direction.

To better gain the insights of the conversion mechanism between the transverse component \mathbf{M}_{ι} and the longitudinal one \mathbf{M}_{z} stemming from tunable m, we show the normalized intensity cross-sections at the focal plane along the x-direction in Figure 2D. The growth and decline of \mathbf{M}_{ι} and \mathbf{M}_{z} , respectively, are observed when m increases from 0 to 2. The intensity of \mathbf{M}_{ι} is a doughnut

shape regardless of the value of m. This is the reminiscent of optical SOC in this optomagnetic process as the transverse component always contains E_z . In contrast, the intensity of \mathbf{M}_z maximizes at the focal point when m=0, and it evolves into a doughnut shape for the cases of m=1, 2, with the diameter of the doughnut being smaller than that of \mathbf{M}_z .

As remarked above, the topological charge effect can be interpreted as that the OAM prescribes how to redistribute the light-induced magnetic energy among different components, the in-plane and out-of-plane ones. Moreover, if $m \neq 0$, SAM and OAM interact with each other; hence, this optical SOC contributes to the ultimate magnetization orientation. Here, we unveil this effect on medium with a specific value of anisotropy, and the influence of the anisotropic properties will be discussed below.

3.2 Influence of materials

3.2.1 Optical anisotropic effect

Next, we emphasize on the properties of the material, particularly on the optical anisotropy and the optomagnetic

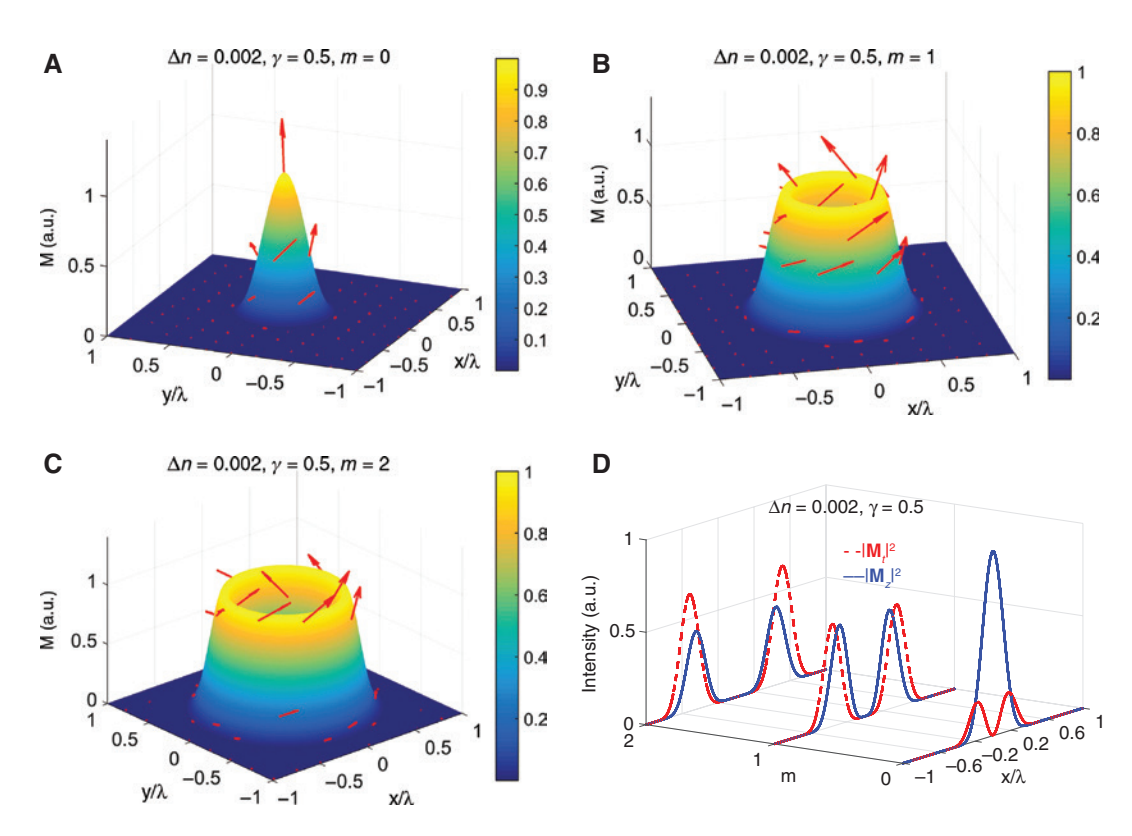


Figure 2: Magnetization pattern influenced by topological charge. (Color online) Topological charge effect on the optically induced magnetization in a medium of $\Delta n = 0.002$ and $\gamma = 0.5$ with topological charge of (A) m = 0, (B) m = 1, and (C) m = 2. The orientation of the magnetization is indicated by arrows. (D) Cross-section of the transverse and longitudinal components for the cases of m = 0, m = 1, and m = 2.

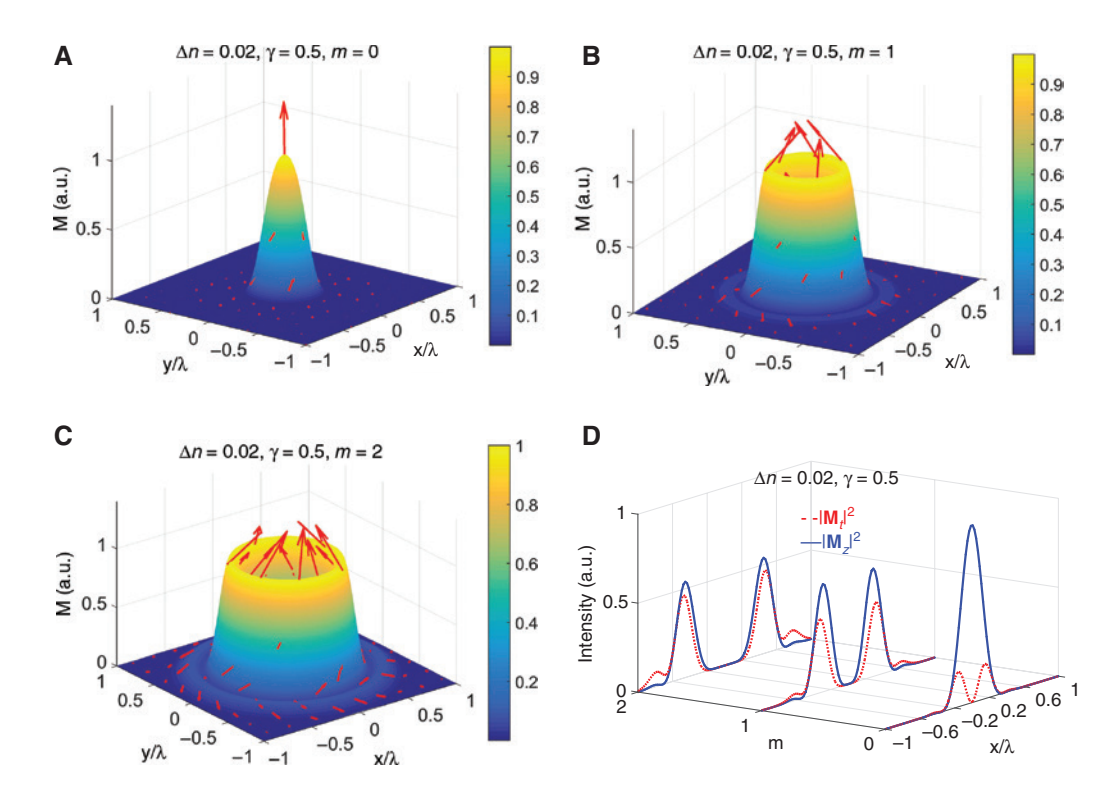


Figure 3: Magnetization pattern influenced by topological charge in a medium with a larger optical anisotropy than that shown in Figure 2. (Color online) Plots of optically induced magnetization in a medium of $\Delta n = 0.02$ and $\gamma = 0.5$ with topological charge of (A) m = 0, (B) m = 1, and (C) m = 2. (D) Cross-section of the transverse and longitudinal components for the cases of m = 0, m = 1, and m = 2.

anisotropy. Phenomenologically, light interacting with magneto-optical material modifies the dielectric tensor of the material and in turn affects the behaviors of the light.

Optical anisotropic effect refers to different responses of the eigenmodes of light upon interaction with birefringent medium. For the axially birefringent medium with small birefringence, the difference appears as a phase factor in the p component of the electric field as demonstrated in Eqs. (1) and (2).

Both intensities of M, and M, of the light-induced magnetization in Figure 3 contain the cases of $\Delta n = 0.02$ with $\gamma = 0.5$ and m = 0, 1, 2. Obviously, we not merely further confirm the topological charge effect but also unravel the optical anisotropic effect in combination with Figures 2 and 3. Together with the case of $\Delta n = 0.002$ with the same values of γ and m discussed above, we find the subtle properties of this optical anisotropic effect. When SOC is absent in the light fields, different Δn has little impact on the magnitude of M, and M. However, the optical anisotropy affects the spatial distribution of the M, component. The larger Δn yields the size of focal distributions of **M**. smaller than those of \mathbf{M}_{z} regardless of the topological charge. Furthermore, compared with the case of $\{m=1,$ $\Delta n = 0.002$ }, the case of {m = 1, $\Delta n = 0.02$ } has the only difference being that it has larger optical anisotropy, in which we see that the birefringence stimulates the transfer of magnetic energy from transverse direction to the vertical direction. This essentially means that Δn can also serve as an effective way to influence the magnetic distribution.

With the assistance of the OAM, however, the effect of birefringence becomes more notable as m increases. Indeed, the modulation by the optical anisotropic effect is especially noticeable for the light with topological charge because of the optical SOC effect. This spin-orbit interaction manifests itself in the transfer of the AM from vortex circularly polarized light to the AM of the material system. Although there is SAM in the circularly polarized light fields, it cannot effectively trigger the redistribution of magnetization in the material system in the absence of OAM. As such, the magnetization can be further affected by the introduction of the optical anisotropy when optical SOC is present. In this way, the optical anisotropic effect offers another degree of freedom to shape the magnetic patterns compared to the previously isotropic studies (see Section 4 of Supplementary Material for more discussions of optical SOC and its implication on the potential applications).

3.2.2 Anisotropic optomagnetic effect

Optically uniaxial anisotropy also results in the tunability of optomagnetic polarization orientation described

by a real symmetric second-rank tensor in transparent medium, which determines the off-diagonal elements of the dielectric tensor. Now, we proceed to analyze the anisotropic optomagnetic effect. Actually, the impact of this effect is straightforward as it relates to the different optomagnetic responses between the transverse and longitudinal directions, as the magnetization intensity distribution and their cross-sections shown in Figure 4.

Nevertheless, this effect deserves as much attention as the other effects demonstrated above. Graphing $|\mathbf{M}_{\perp}|^2$ and $|\mathbf{M}|^2$ versus γ as illustrated in Figure 4D, we find the clear trends as anticipated. The magnetic energy density distribution strongly depends on the anisotropic optomagnetic effect. We already know that when there is helical phase in the light fields the induced **M** will eventually evolve into a doughnut profile. However, for material with large (such as $\gamma = 0.1$) optomagnetic response in the in-plane direction, M, becomes dominant and makes the intensity pattern doughnut shaped, thus creating a dark channel in the focal area. On the other side, for a given *m* and Δn , when γ is large enough, \mathbf{M}_{\perp} plays a dominant role, which brings about a bright channel in the focal region; apparently, there should be a range of γ values being able to balance these two components.

Note that although this anisotropic optomagnetic effect is crucial for the polarization orientation and the pattern of the magnetic domain, it can certainly not change the number of the discrete magnetic states printed by different m values in the same system (with the same Δn); for the topological charge effect and the optical anisotropic effect, however, they not merely change the polarization orientation and the pattern of individual magnetic state but also considerably alter the relative polarization orientations of the diverse magnetic states. This has significant implications for the optomagnetic applications, which will be discussed below.

4 Optomagnetic applications

4.1 3D optomagnetic recording

Putting together all the findings in the preceding section, it is clearly seen that the choices of the phase of the incident light fields, the optical anisotropy, and the anisotropic optomagnetic response of the medium jointly contribute to the magnetization patterns in the focal region. This

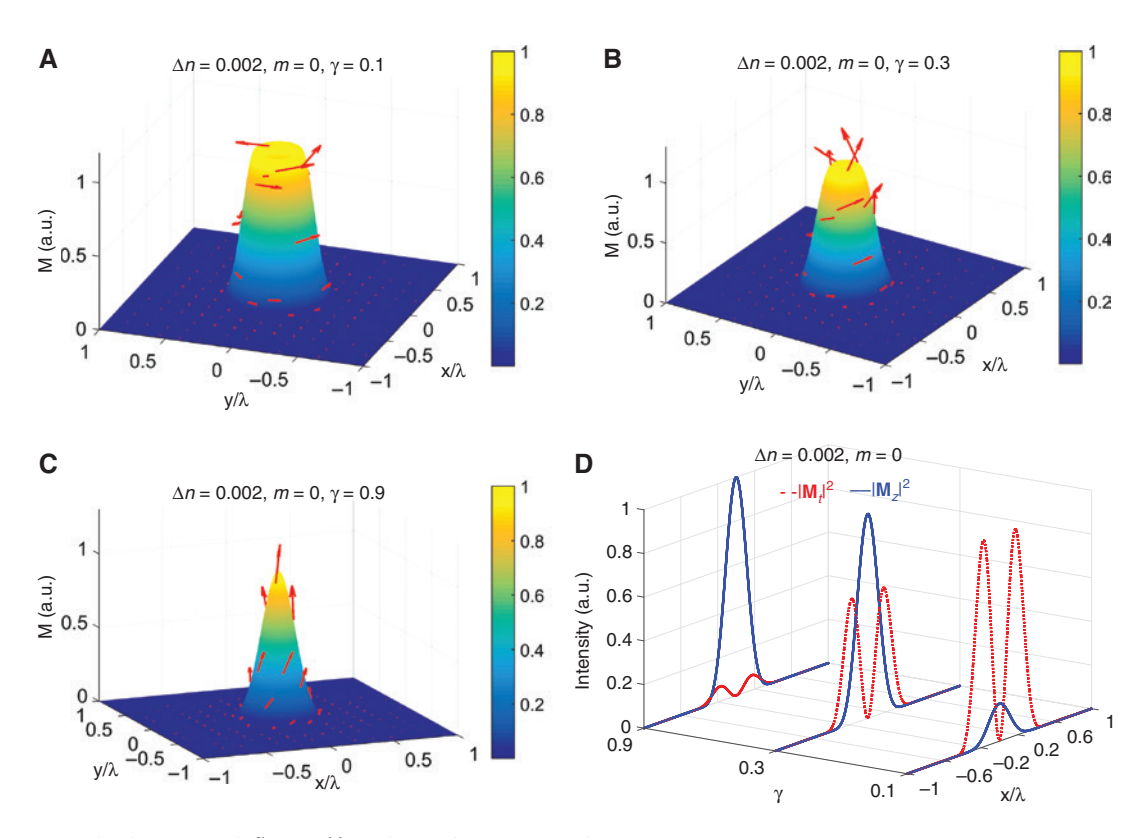


Figure 4: Magnetization pattern influenced by anisotropic optomagnetic response. (Color online) Anisotropic optomagnetic effect on the optically induced magnetization in a medium of $\Delta n = 0.002$ and m = 0 with anisotropic optomagnetic response of (A) $\gamma = 0.1$, (B) $\gamma = 0.3$, and (C) $\gamma = 0.9$. (D) Cross-section of the transverse and longitudinal components for the cases of $\gamma = 0.1$, $\gamma = 0.3$, and $\gamma = 0.9$.

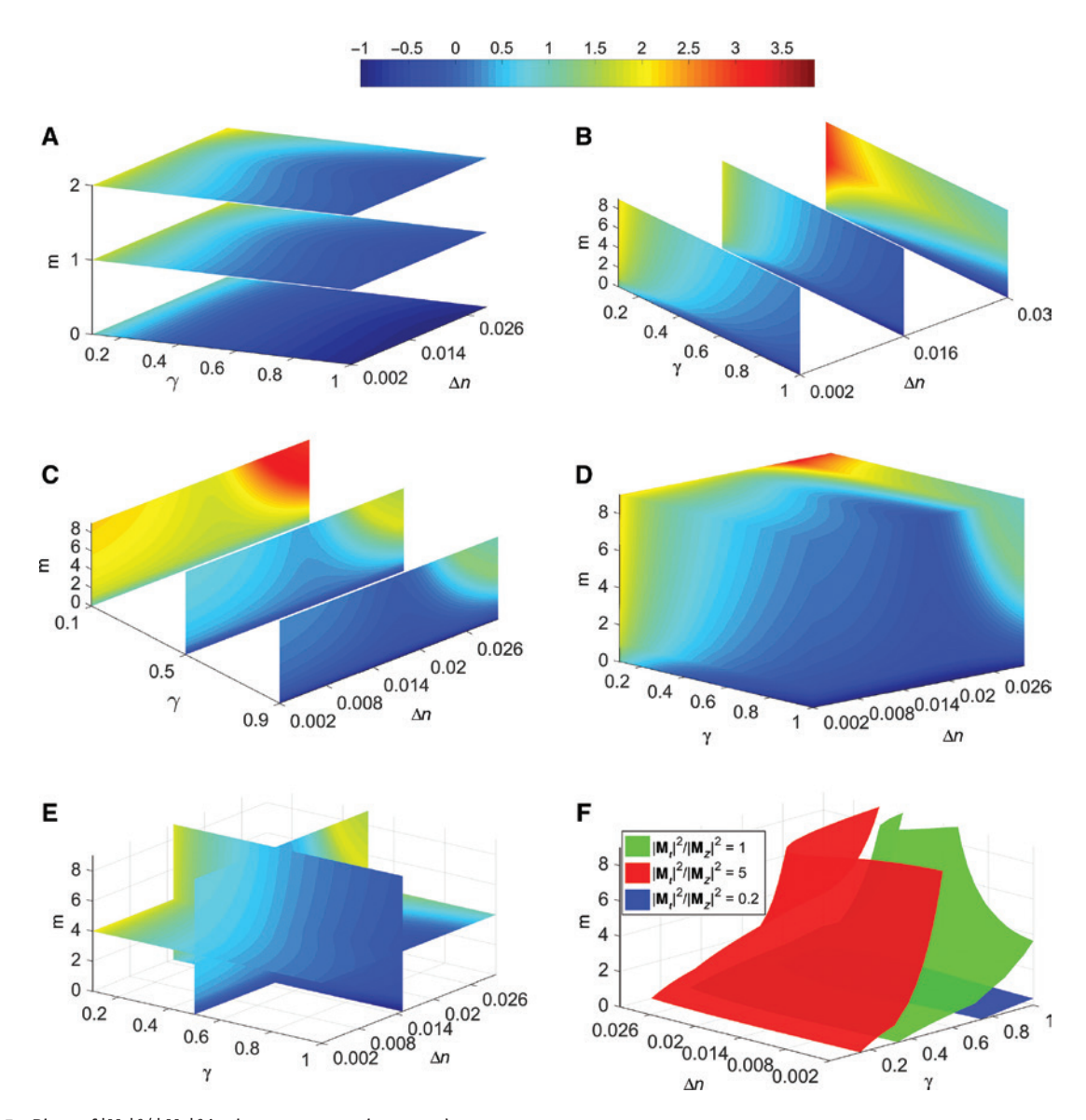


Figure 5: Plots of $|\mathbf{M}_t|^2/|\mathbf{M}_z|^2$ in the parameter planes and space. (Color online) Magnetization distributions in (A) 2D Δn - γ parameter plane, (B) 2D m- γ parameter plane, (C) 2D Δn -m parameter plane, and (D) 3D Δn - γ -m parameter space. (E) Distributions inside the Δn - γ -m parameter space. The value of $|\mathbf{M}_t|^2/|\mathbf{M}_z|^2$ presented in (A–E) is a \log_{10} scale. (F) Three isosurfaces representing three different configurations: the longitudinally dominated, the transversally dominated, and the longitudinal and transverse balanced cases.

optically induced magnetization, as a vector quantity, has been shown to be controllable as a function of the tuning parameters related to both the light fields and the magneto-optical materials. Indeed, all these three degrees of freedom together with the optical SOC mechanism have remarkable impact on the magnetization orientation.

The fact that the arbitrary orientation of magnetization can be realized in this system implies that it has huge potentials in high-density 3D optomagnetic recording application. To have a comprehensive view of this light-and material-mediated magnetization control, it is instructive to devote this section to analyze the magnetization in

the light-material parameter space. The intensity ratio of \mathbf{M}_t to \mathbf{M}_z , $|\mathbf{M}_t|^2/|\mathbf{M}_z|^2$, can be viewed as an indicator of the magnetic energy density distribution during the optomagnetic process. With respect to this ratio, we can directly read information from the light-material parameter space. For example, all the points (corresponding to some light fields and materials) in this parameter space with the relation $\log_{10}(|\mathbf{M}_t|^2/|\mathbf{M}_z|^2) \sim 0$ may be used to perform 3D all-optical magnetic recording with the orientation of \mathbf{M} directing between \mathbf{M}_t and \mathbf{M}_z ; if $\log_{10}(|\mathbf{M}_t|^2/|\mathbf{M}_z|^2)$ is large/small enough compared to 0, those points relate to horizontal/longitudinal magnetic recording.

First, we present in Figure 5A the resulting magnetization distribution when Δn and γ change simultaneously. In this case, the material dependence of $|\mathbf{M}_{\perp}|^2 / |\mathbf{M}_{\perp}|^2$ suggests that the impact resulting from the anisotropic optomagnetic effect is considerably stronger than that from the optical anisotropic effect. When γ changes from 0.1 to 1, the magnetization is switched from transverse to longitudinal direction. In this way, the anisotropic optomagnetic responses directly influence the direction of M. As for the optical anisotropic effect, M experiences minor changes as Δn varies, which means that the optical anisotropic effect affects mainly on the magnitude of M. However, the topological charge of the illuminating light also plays an important role in the behaviors of **M** as expected. The role of the optical anisotropic effect would drastically grow in importance when m increases, as shown in Figure 5A for cases of m = 0, 1, 2. For m = 0, the overall feature of the optical anisotropic dependence does not change significantly with fixed γ . Consequently, γ is the principal factor that needs to be taken into account; for m=1 or 2, however, the overall character of the Δn dependence displays more complex behaviors due to the optical SOC in the anisotropic medium. Hence, γ is not the unique element pertinent to the all-optical magnetic recording, but Δn must be considered as well. In these cases, every γ corresponds to different magnetization distributions depending on the value of Δn .

Similarly, we plot $|\mathbf{M}_{\epsilon}|^2 / |\mathbf{M}_{\epsilon}|^2$ versus both γ and m in Figure 5B for three different Δn values. We can easily find out the magnetization distribution in these 2D $m - \gamma$ parameter planes. As shown in this diagram for $\Delta n = 0.002$, $\Delta n = 0.016$, and $\Delta n = 0.03$, we observe the longitudinaldominated magnetization distribution on the lower right corner of these planes but the transverse-preferred pattern on their top left side.

Further, we graph $|\mathbf{M}_{\perp}|^2 / |\mathbf{M}_{\perp}|^2$ in the $m - \Delta n$ plane in Figure 5C for three different γ values. Obviously, all these figures show the same patterns, but they differ in their magnitudes. For example, the smaller value $\gamma = 0.1$ provides more choices for the horizontal component being dominant, whereas the limiting case $\gamma = 1$ offers more solutions for a dominant vertical one.

Ultimately, as a full view of our method, we make all degrees of freedom contribute to the formation of the magnetization pattern. A "dictionary" can be constructed by taking all the tuning parameters from light fields and materials into account. We map the magnetization distribution onto the 3D parameter space spanned by $\{m, \Delta n, \gamma\}$, as shown in Figure 5D and E. Actually, it again confirms our results demonstrated in the previous sections. One can easily look up the "dictionary" for the suitable light fields and materials for 3D optomagnetic recording.

Remarkably, if one wants to have a specific **M**, there is absolutely not a unique candidate of light-material system (a selective combination of $\{m, \Delta n, \gamma\}$) for it, but generally multiple alternatives due to the reciprocal cooperation among m, Δn , and γ . This multivalued property is intriguing in our theoretical framework. In Figure 5F, three different configurations corresponding to the longitudinally dominated, transversally dominated, and longitudinal and transverse balanced cases are presented. They are $|\mathbf{M}_{\perp}|^2/|\mathbf{M}_{\perp}|^2=0.2$, 5, and 1, respectively. In this 3D parameter space, the overall trends can be clearly seen by these three isosurface pictures. More specifically, the isosurface with $|\mathbf{M}_{\perp}|^2/|\mathbf{M}_{\perp}|^2=5$ verifies our analysis above, as is shown that every m ranging from 0 to 9 can achieve a transverse pattern provided the appropriate Δn and γ . However, since we only consider the cases with $\gamma \leq 1$, which means that the optomagnetic response in the transverse direction is larger than that in the longitudinal direction, in this parameter space, only m=0 and 1 may give rise to the longitudinally dominant configurations. Focusing on the Δn parameter, again taking $|\mathbf{M}_{\perp}|^2/|\mathbf{M}_{\perp}|^2=5$ as an example, every birefringence of $\Delta n \leq 0.03$ has its position on this isosurface but depending both on the values of m and γ . There are many candidates, i.e. different combinations of $\{m, \Delta n, \gamma\}$, and one can obtain the expected magnetization state unequivocally, offering multiple routes to flexibly control over the desired magnetization state by allying the phase polarization configured optical fields with the existent anisotropic magneto-optical materials. Thus, in our strategy, the multivalued property is instrumental in the discovery of promising solutions in 3D optomagnetic recording.

4.2 All-optical multistate magnetization

Besides the optomagnetic recording application inspired by the 3D magnetization generation, an all-optical multistate memory device can be conceived through such a single optically configured vectorial beam system. In Figure 6A, the impact of the topological charge on the magnetization distribution is presented by considering the cases of different γ with fixed Δn and different Δn with fixed γ . Interestingly, compared to the cases of $\gamma = 0.1$ and 5, which always have the dominant transverse and longitudinal magnetic states, respectively, we find that the magnetic state depends on the values of *m* when $\gamma = 0.5$. Explicitly, m=0 yields a longitudinal magnetic state, m=1 leads to the longitudinal component approximately

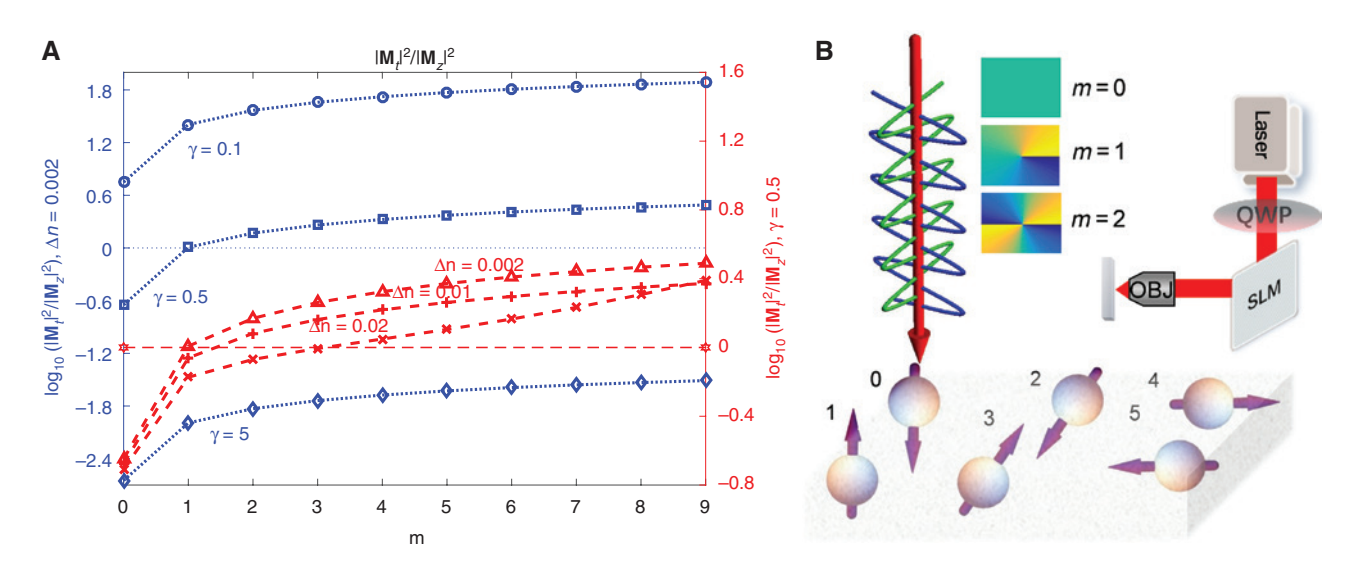


Figure 6: Illustration of the idea of all-optical multistate magnetization, and schematic of its realization. (Color online) (A) Optically induced magnetic energy density as a function of m for configurations of three different γ values, $\gamma = 0.1$, 0.5, and 5, and three different Δn values, $\Delta n = 0.002$, 0.01, and 0.02. (B) Scheme for the generation of all-optical multistate magnetization using circularly polarized vortex light. The top right corner shows the schematic of the optical setup system. The linearly polarized light emitted from the laser is converted into the circularly polarized one by the quarter wave plate (QWP). The SLM encodes phase into the light with m = 0, m = 1, or m = 2. Then, the light is focused by the objective (OBJ) into the uniaxial material.

equating the transverse one, and m=2 brings out a transversely dominated state. These results provide us with profound insights into the control of multistate magnetization in the same material system, such as the material characterized by $\Delta n = 0.002$ and $\gamma = 0.5$. We further specify the influence of Δn , and a closer inspection is shown in Figure 6A as well (for other configurations of multistate magnetization in terms of birefringence and optomagnetic response, see Section 3 of Supplementary Material). As the birefringence increases, the transverse component tends to gain more magnetic energy than the longitudinal counterpart. Hence, we can exploit this intriguing fact to create multilevel magnetization in some birefringent materials.

As a conceptual illustration, we construct a senary prototype system consisting of six-orientation magnetic states with a sequence of a single light pulse impinging into the material, for example, with optical anisotropy Δn =0.002 and anisotropic optomagnetic response γ =0.5. These different states can be obtained by tuning the topological charge of the tailored light. We exhibit this memory paradigm in Figure 6B. As revealed before, m=0 induces the "up" or "down" states (0 or 1), m=1 induces the oblique states (2 or 3), and m=2 induces the in-plane ones (4 or 5). These six states represented as from 0 to 5 can be used for a digit of a senary (base 6) numeral system. To rearrange the order of the senary digits, one could modulate the polarization and the phase structure of the incident light. In other words, tuning the topological charge from 0 to 2

rotates the magnetic state accordingly, and changing the helicity (circular polarization state) may lead to the switching of these states. In this prototypical example, we show its attractive potential in the optomagnetic recording. The lateral and the axial full-width at half-maximum of a beam, such as an m = 0 beam, are 0.36 λ and 0.51 λ , respectively, in the tight focusing system. With the focal volume approximately $0.27\lambda^3$, the theoretical volumetric storage density of about 600 Tbit/in³ at $\lambda = 800$ nm could be achievable. Furthermore, nowadays, the spatial light modulator (SLM) can reach a limit of 256 gray levels. It has significant advantage over the present-day storage techniques [47], as the volumetric storage density could, in theory, be two orders of magnitude higher, up to $10^3 \sim 10^4$ Tbit/in³. Despite the prospect presented, the efficiency of the magnetic vector control and the efficient detection of the 3D multistate magnetization could be the challenges confronted in experimental practice.

The multistate magnetization derives from the interaction between structured light and uniaxial material with desirable optical and optomagnetic response. Intriguingly, it is achievable in an all-optical way. In principle, more states can be produced, and if we further optimize the polarization, phase, and amplitude of the light fields, such multistate magnetization can be better realized. Thereby, this system has great potentials in multinary data storage and information multiplexing. The state-of-theart strategies for the generations of multilevel magnetic

states mainly use the external magnetic or electric field in magnetic multilayer, multiferroic material, artificial ferromagnetic/ferroelectric heterostructure systems [8, 48, 49]. Some uses light to control the carrier in materials, which relies on the detailed magnetic structures such as the fourfold magnetic anisotropy in (Ga,Mn)As [50], and to use the light-induced spin-polarized currents in the magnetic spin-valve structure ([Co/Pt]/Cu/GdFeCo) [51]. Therefore, in contrast to the current methods, the benefits of this all-optical way are the flexibility, efficiency, and repeatability, as it is very easy to engineer the light beam for optimum performance; nowadays, the time scales of laser can reach down to the femtosecond range. Importantly, these multifold possible orientations of the magnetic state may greatly increase the recording density by writing multibits at one spot. As a result, the all-optical multistate could advance the development in data storage and memories, cryptography, and information processing technologies, and it may also find applications in digital holography and the detection of magnetic particles.

5 Conclusion

In conclusion, we uncover the topological charge effect, the optical anisotropic effect, and the anisotropic optomagnetic effect in the optomagnetic system and therefore establish the relationship between the magnetization pattern and the properties of the incoming circularly polarized vortex light and the anisotropic medium, in which the anisotropy-mediated SOC mechanism plays an important role. A full picture is presented to search for the tunable spatial distribution of magnetic energy density induced by the IFE in a single optically configured focusing system. Most importantly, in this optomagnetical platform, the 3D optomagnetic recording and all-optical multistate memory device can be conceptually realized, and the possible lightmaterial systems to fulfill specific magnetization configurations are also predicted. Hence, we deliver an all-optical method to vectorially control the multistate magnetization patterns transversely, longitudinally, or 3D by appropriately tuning the structured light fields and the material with anisotropic properties. We believe that our findings will help better understand the light-matter interaction and provide theoretical guidelines and inspire new ideas in the search for natural or even designing artificial materials for the potential optomagnetic applications.

On the one hand, the light-magnetic system consisting of controllable degree of freedoms shed light on the field of magnetization dynamics and especially in the ultrafast domain [13, 52, 53]. The mechanism of the exchange of energy and AM between the light fields and magnetic systems may be uncovered by the phenomena resulting from the photonic SOC, specific magnetic properties, and their intricate interactions. On the other hand, being able to yield 3D polarized orientations of magnetization and even multilevel magnetic states in a single optically configured focusing system, it provides a new way toward multinary recording, thus achieving high data storage capacity by encoding information in the multidimensional space. At the same time, with different physical processes available in this system, multiplexing of a variety of data channels can be created. In such an optomagnetic interaction based system, the encryption and decryption of the data rely on the optomagnetic and magneto-optical mechanisms, thereby providing a new type of security different from those relying on the mathematical or quantum-mechanical methods.

Acknowledgments: The authors thank the National Natural Science Foundation of China (grant nos. 11675014, 11604236, 61575139, and 11974258, Funder Id: http:// dx.doi.org/10.13039/501100001809). S.L. is grateful to the China Scholarship Council (grant no. 201606030283, Funder Id: http://dx.doi.org/10.13039/501100004543). B.J. acknowledges support from the Australia Research Council through the Discovery Project Scheme (DP190103186) and the Industrial Transformation Training Centres Scheme (grant no. IC180100005).

References

- [1] Kimel A, Kirilyuk A, Usachev P, Pisarev R, Balbashov A, Rasing T. Ultrafast non-thermal control of magnetization by instantaneous photomagnetic pulses. Nature 2005;435:655-7.
- Stanciu C, Hansteen F, Kimel A, et al. All-optical magnetic recording with circularly polarized light. Phys Rev Lett 2007;99:047601.
- [3] Le Guyader L, El Moussaoui S, Buzzi M, et al. Deterministic character of all-optical magnetization switching in GdFe-based ferrimagnetic alloys. Phys Rev B 2016;93:134402.
- [4] Stupakiewicz A, Szerenos K, Afanasiev D, Kirilyuk A, Kimel A. Ultrafast nonthermal photo-magnetic recording in a transparent medium. Nature 2017;542:71-4.
- [5] Rozenberg M, Inoue I, Sanchez M. Nonvolatile memory with multilevel switching: a basic model. Phys Rev Lett 2004;92:178302.
- [6] Guo Y, Di C-A, Ye S, et al. Multibit storage of organic thin-film field-effect transistors. Adv Mater 2009;21:1954-9.
- [7] Lee D, Yang SM, Kim TH, et al. Multilevel data storage memory using deterministic polarization control. Adv Mater 2012;24:402-6.
- Zhong H, Wen Y, Zhao Y, et al. Ten states of nonvolatile memory through engineering ferromagnetic remanent magnetization. Adv Funct Mater 2018;29:1806460.

- [9] Pitaevskii L. Electric forces in a transparent dispersive medium. Sov Phys JETP 1961;12:1008-13.
- [10] Pershan P. Nonlinear optical properties of solids: energy considerations. Phys Rev 1963;130:919.
- [11] Van der Ziel J, Pershan P, Malmstrom L. Optically-induced magnetization resulting from the inverse Faraday effect. Phys Rev Lett 1965;15:190.
- [12] Pershan P, Van der Ziel J, Malmstrom L. Theoretical discussion of the inverse Faraday effect, Raman scattering, related phenomena. Phys Rev 1966;143:574.
- [13] Kirilyuk A, Kimel AV, Rasing T. Ultrafast optical manipulation of magnetic order. Rev Mod Phys 2010;82:2731.
- [14] Kalashnikova AM, Kimel AV, Pisarev RV. Ultrafast opto-magnetism. Phys Uspekhi 2015;58:969.
- [15] Nie Z-Q, Lin H, Liu X-F, et al. Three-dimensional super-resolution longitudinal magnetization spot arrays. Light Sci Appl 2017:6:e17032.
- [16] Hao C, Nie Z, Ye H, et al. Three-dimensional supercritical resolved light-induced magnetic holography. Sci Adv 2017;3:e1701398.
- [17] Wang S, Cao Y, Li X. Generation of uniformly oriented in-plane magnetization with near-unity purity in 4π microscopy. Opt Lett 2017:42:5050-3.
- [18] Kanda N, Higuchi T, Shimizu H, Konishi K, Yoshioka K, Kuwata-Gonokami M. The vectorial control of magnetization by light. Nat Commun 2011;2:362.
- [19] Satoh T, Iida R, Higuchi T, Fiebig M, Shimura T. Writing and reading of an arbitrary optical polarization state in an antiferromagnet. Nat Photonics 2015;9:25-9.
- [20] Yan W, Nie Z, Liu X, Zhang X, Wang Y, Song Y. Creation of isotropic super-resolved magnetization with steerable orientation. APL Photonics 2018;3:116101.
- [21] Wang S, Luo J, Zhu Z, et al. All-optical generation of magnetization with arbitrary three-dimensional orientations. Opt Lett 2018;43:5551-4.
- [22] Volkov P, Novikov M. Inverse Faraday effect in anisotropic media. Crystallogr Rep 2002;47:824-8.
- [23] Shen Y-R. The Principles of nonlinear optics. New York: Wiley-Interscience, 1984:575.
- [24] Popova D, Bringer A, Blügel S. Theoretical investigation of the inverse Faraday effect via a stimulated Raman scattering process. Phys Rev B 2012;85:094419.
- [25] Battiato M, Barbalinardo G, Oppeneer PM. Quantum theory of the inverse Faraday effect. Phys Rev B 2014;89:014413.
- [26] El Hadri MS, Hehn M, Malinowski G, Mangin S. Materials and devices for all-optical helicity-dependent switching. J Phys D Appl Phys 2017;50:133002.
- [27] Němec P, Fiebig M, Kampfrath T, Kimel AV. Antiferromagnetic opto-spintronics. Nat Phys 2018;14:229-41.
- [28] Bossini D, Belotelov V, Zvezdin A, Kalish A, Kimel A. Magnetoplasmonics and femtosecond optomagnetism at the nanoscale. ACS Photonics 2016;3:1385-400.
- [29] Jin Z, Ma H, Wang L, Ma G, Guo F, Chen J. Ultrafast alloptical magnetic switching in NaTb(WO,)2. Appl Phys Lett 2010;96:201108.
- [30] Satoh T, Van Aken BB, Duong NP, Lottermoser T, Fiebig M. Ultrafast spin and lattice dynamics in antiferromagnetic Cr₂O₃. Phys Rev B 2007;75:155406.
- [31] Ebert H. Magneto-optical effects in transition metal systems. Rep Prog Phys 1996;59:1665.
- [32] Ferré J, Gehring G. Linear optical birefringence of magnetic crystals. Rep Prog Phys 1984;47:513.

- [33] Osgood R III, Riggs K, Johnson AE, Mattson J, Sowers C, Bader S. Magneto-optic constants of hcp and fcc Co films. Phys Rev B 1997;56:2627.
- [34] Arregi JA, Riego P, Berger A. What is the longitudinal magnetooptical Kerr effect? J Phys D Appl Phys 2016;50:03LT01.
- [35] Weller D, Harp G, Farrow R, Cebollada A, Sticht J. Orientation dependence of the polar Kerr effect in fcc and hcp Co. Phys Rev Lett 1994;72:2097.
- [36] Arregi J, González-Daz J, Soriano N, Mora B, Berger A. Surfacetopography induced optical and magneto-optical anisotropy of permalloy gratings. J Phys D Appl Phys 2015;48:305002.
- [37] Richards B, Wolf E. Electromagnetic diffraction in optical systems, II. Structure of the image field in an aplanatic system. Proc R Soc Lond Ser A Math Phys Sci 1959;253:358-79.
- [38] Boivin A. Wolf E. Electromagnetic field in the neighborhood of the focus of a coherent beam. Phys Rev 1965;138:B1561.
- [39] Zhan Q. Cylindrical vector beams: from mathematical concepts to applications. Adv Opt Photonics 2009;1:1-57.
- [40] Gu M. Advanced optical imaging theory. Berlin Heidelberg, Germany, Springer Science & Business Media, 2000;75.
- [41] Stallinga S. Axial birefringence in high-numerical-aperture optical systems and the light distribution close to focus. JOSA A 2001;18:2846-59.
- [42] Birss RR. Symmetry and magnetism. Amsterdam: North-Holland, 1964;863.
- [43] Marrucci L, Manzo C, Paparo D. Optical spin-to-orbital angular momentum conversion in inhomogeneous anisotropic media. Phys Rev Lett 2006;96:163905.
- [44] Devlin RC, Ambrosio A, Rubin NA, Mueller JB, Capasso F. Arbitrary spin-to-orbital angular momentum conversion of light. Science 2017;358:896-901.
- [45] Zhao Y, Edgar JS, Jeffries GD, McGloin D, Chiu DT. Spin-toorbital angular momentum conversion in a strongly focused optical beam. Phys Rev Lett 2007;99:073901.
- [46] Bliokh KY, Ostrovskaya EA, Alonso MA, Rodrguez-Herrera OG, Lara D, Dainty C. Spin-to-orbital angular momentum conversion in focusing, scattering, and imaging systems. Opt Express 2011;19:26132-49.
- [47] Fontana R Jr, Decad G, Hetzler S. Volumetric density trends (TB/ in.3) for storage components: TAPE, hard disk drives, NAND, and Blu-ray. J Appl Phys 2015;117:17E301.
- [48] Wei Y, Gao C, Chen Z, et al. Four-state memory based on a giant and non-volatile converse magnetoelectric effect in FeAl/PIN-PMN-PT structure. Sci Rep 2016;6:30002.
- [49] Zhao X, Wen J, Yang B, et al. Electric field manipulated multilevel magnetic states storage in FePt/(011) PMN-PT heterostructure. ACS Appl Mater Interfaces 2017;9:36038-44.
- [50] Astakhov GV, Kimel AV, Schott GM, et al. Magnetization manipulation in (Ga,Mn) as by subpicosecond optical excitation. Appl Phys Lett 2005;86:152506.
- [51] Iihama S, Xu Y, Deb M, et al. Single-shot multi-level all-optical magnetization switching mediated by spin transport. Adv Mater 2018;30:1804004.
- [52] Steil D, Alebrand S, Hassdenteufel A, Cinchetti M, Aeschlimann M. All-optical magnetization recording by tailoring optical excitation parameters. Phys Rev B 2011;84:224408.
- [53] Satoh T, Terui Y, Moriya R, et al. Directional control of spin-wave emission by spatially shaped light. Nat Photonics 2012;6:662.

Supplementary Material: The online version of this article offers supplementary material (https://doi.org/10.1515/nanoph-2019-0198).